Reevaluating how charged particles cause space weathering on airless bodies

A. P. Jordan[a,b,*]

[a] *Institute for the Study of Earth, Oceans, and Space, University of New Hampshire, Durham, New Hampshire, USA.*
[b] *Solar System Exploration Research Virtual Institute, NASA Ames Research Center, Moffett Field, California, USA.*

Abstract

Many experiments have attempted to simulate how charged particles cause space weathering on airless bodies throughout the Solar System. Researchers have typically applied these experimental results by assuming that high laboratory fluxes cause the same effects as do the significantly lower fluxes found in nature. New work, however, shows that this assumption may often be invalid. In particular, experiments using charged particle fluences $\gtrsim 10^{10}$ cm^{-2} without adequate steps to neutralize the targets risk causing dielectric breakdown, or "sparking"—a process that may affect some airless bodies. Consequently, it is critical to understand the laboratory conditions under which breakdown occurs, both to ensure that experiments properly simulate the effects of charged particles and to study the possibility that dielectric breakdown can, in some locations, contribute to space weathering.

Keywords: Solar wind, Regoliths, Moon, surface, Asteroids, surfaces, Jupiter, satellites

---

1. Introduction

Airless bodies throughout the Solar System are exposed to a range of space weathering processes, such as meteoroid impacts, plasmas, and ionizing radiation (e.g., see the review by Pieters and Noble (2016)). These processes must be understood in order to interpret remote sensing observations and returned samples. In particular, weathering by charged particles has been

* *Corresponding author address:* Morse Hall Rm. 106A, 8 College Rd., Durham, NH 03824 USA.

Email address: a.p.jordan@unh.edu (A. P. Jordan)

simulated in many experiments designed to study sputtering, amorphization, and radiolysis on bodies like the Moon, asteroids, icy satellites, and comets (Table 1).

In applying the results of these experiments, researchers generally assume that the critical factor is the fluence of charged particles. Experiments must deposit these fluences in reasonable timescales; thus, they use fluxes that are many orders of magnitude higher than those found in natural environments. Growing evidence, however, shows that such fluxes alter materials in ways that either may not apply to the body in question or may apply in unexpected ways. In particular, I show below that the experiments listed in Table 1 use fluxes and fluences that are known to cause dielectric breakdown (or "sparking") in electrically insulating materials. Consequently, it is necessary to reevaluate these experiments and how they apply to space weathering on airless bodies throughout the Solar System.

Target	**Particles**	**Max. flux (cm^{-2} s^{-1})**	**Max. fluence (cm^{-2})**	**Reference**
		Moon		
Rocks, rock powder	2 keV H^+	$\sim 10^{16}$	$\sim 10^{21}$	Hapke (1965)
Rock powder	2 keV H^+	$\sim 3 \times 10^{15}$	2.5×10^{20}	Hapke (1968)
Pulverized lunar rock	2 keV H^+	Not stated	$\sim 10^{20}$	Hapke et al. (1970)
Terrestrial & lunar igneous rock powder	2 keV H^+	$\sim 2 \times 10^{15}$	$\sim 10^{20}$	Hapke (1973)
"Lunarlike glass"	2 keV H^+	$\sim 10^{15}$	Not stated	Cassidy and Hapke (1975)
Lunar rocks	2 keV H^+ & He^+	$\sim 10^{15}$	Not stated	Hapke et al. (1975)

Olivine (breakdown)	30 keV e^-	3.7×10^{15}	3.5×10^{18}	Lemelle et al. (2003)
Lunar basalt	1 MeV Kr^+	Not stated	9×10^{15}	Christoffersen and Keller (2007)
Olivine, ilmenite	50 keV He^+	$\lesssim 1 \times 10^{14}$	5×10^{16}	Zhu et al. (2014)
Lunar basalt	1 keV H^+	$\sim 3.55 \times 10^{12}$	6.4×10^{16}	Shusterman et al. (2020)
		Asteroids		
Olivine	1 keV H^+, 4 keV He^+	6×10^{13}	1×10^{18}	Dukes et al. (1999)
Olivine powder	4 keV He^+	$\sim 1.4 \times 10^{13}$	3.1×10^{18}	Loeffler et al. (2009)

Various silicates	50 keV He^+	$\lesssim 1 \times 10^{14}$	5×10^{16}	Fu et al. (2012)
Allende meteorite	40 keV He^+ & Ar^+	$\sim 1 \times 10^{12}$	$\sim 1 \times 10^{16}$	Brunetto et al. (2014)
Murchison meteorite	40 keV He^+ & Ar^+	Not stated	3×10^{16}	Lantz et al. (2015)
Olivine	$10-50$ keV H_2^+, $4-50$ keV He^+	2.7×10^{13}	1×10^{18}	Matsumoto et al. (2015)
Silicates, meteorites	40 keV He^+	Not stated	6×10^{16}	Lantz et al. (2017)
For a list of further experiments focused on asteroids, see Table 1 in Kanuchova et al. (2015)				
		Io		
Sulfur (breakdown)	$10-30$ keV electrons	$\sim 10^{12}$	$\sim 10^{15}$	Campins and Krider (1989)
		Water Ice		

Crystalline water ice	100 keV e^-	Not stated	$> 2 \times 10^{17}$	Lepault et al. (1983)
Crystalline & amorphous water ice	$100 - 200$ keV e^-	1×10^{17}	6×10^{17}	Heide (1984)
Water and C_6H_6 ice	$3 - 100$ keV Ar^+	Not stated	1.6×10^{16}	Strazzulla et al. (1991)
Crystalline & amorphous water ice	100 keV H^+ & Ar^+	Not stated	2.7×10^{15}	Baragiola et al. (2005)
Crystalline & amorphous water ice (breakdown)	100 keV Ar^+	Not stated	$\sim 2.4 \times 10^{16}$	Baragiola et al. (2008)
Crystalline & amorphous water ice	225 keV H^+	$\lesssim 10^{12}$	3.8×10^{15}	Famá et al. (2010)

Amorphous water ice (breakdown)	100 keV Ar^+	7.8×10^{11}	Not stated	Shi et al. (2010)
Crystalline & amorphous water ice (breakdown)	$1 - 200$ keV Ar^+	7.8×10^{11}	Not stated	Shi et al. (2012)
Amorphous water ice	$0.1 - 2$ keV e^-	1.0×10^{13}	$\sim 3 \times 10^{15}$	Barnett et al. (2012)
Pure & salty water ice	$10 - 25$ MeV e^-	$\sim 1 \times 10^{13}$	$\sim 1 \times 10^{16}$	Henderson et al. (2019)
Water ice	$0.5 - 10$ keV e^-	$1 - 11 \times 10^{13}$	$\sim 5 \times 10^{17}$	Meier and Loeffler (2020)
Water ice	$1 - 10$ keV e^-	Not stated	2.32×10^{17}	Loeffler et al. (2020)

Microporous amorphous water ice	5 keV e^-	$\sim 2 \times 10^{12}$	1.1×10^{15}	Behr et al. (2020)
		Formation of OH/H_2O on the Moon		
Soda-lime-silicate glass	0.5, 1 Mev H^+	Not stated	7×10^{17}	Zeller et al. (1966)
Silica glasses	13 keV H^+, 17.5 keV He^+	Not stated	5×10^{18}	Yoshida et al. (2004)
Olivine & SiO_2 powders	3 keV D^+	$\sim 5 \times 10^{15}$	$\sim 10^{18}$	Managadze et al. (2011)
Highland & mare soils	2.2 keV H_2^+, D_2^+	$\sim 10^{13}$	$\sim 10^{17}$	Ichimura et al. (2012)
Olivine, clinopyroxene, anorthite	5 keV H^+, He^+	Not stated	1.0×10^{19}	Bradley et al. (2014)

Olivine	5 keV D_2^+	2×10^{13}	1.0×10^{18}	Zhu et al. (2019)

Table 1: Sampling of experiments that used charged particles to irradiate materials found on airless bodies. Experiments that explicitly studied dielectric breakdown are labeled.

2. Revisiting space weathering experiments

Charged particle experiments typically assume that fluence, and not flux, determines how a target material changes. Yet new research is showing that flux also plays a role; high experimental fluxes can alter materials in ways that do not occur in lower flux environments. This difference between the laboratory and most environments in our Solar System makes it critical to understand the limitations of particle experiments and to revisit how they have affected our understanding of space weathering.

An example of this disparity is the space weathered rims that form on regolith grains on the Moon and asteroids. These thin (less than a couple hundred nm) rims grow via two main processes: vapor deposition and solar wind amorphization (Keller and McKay, 1997; Keller et al., 2021). Charged particle experiments also create amorphized rims, seemingly simulating the space weathering caused by the solar wind (e.g., Bibring et al., 1975; Dukes et al., 1999; Carrez et al., 2002; Loeffler et al., 2009).

When extrapolated to the Moon and asteroids, however, these experiments predict that space weathered rims should form orders of magnitude faster than what is observed. A ~ 50 nm rim should form on a plagioclase grain in ~ 500 yr at 1 AU, but analyses have shown this thickness (on anorthite) requires ~ 2 Myr (Keller et al., 2021). Rims on olivine should form about as quickly as on plagioclase (e.g., Poppe et al., 2018), but here the disagreement is greater. Olivine grains from the Moon and asteroid 25143 Itokawa have damaged rims, but none have amorphous rims, even though some have been exposed to the solar wind for up to ~ 20 Myr (Christoffersen et al., 2020; Keller et al., 2021).

In the case of olivine, it seems that solar wind fluxes are low enough to allow olivine to recover in a way that the high experimental fluxes do not allow (Christoffersen et al., 2020). It is unclear if this is also the case with the anorthite grains, since plagioclase should not be resistant to radiation damage (Keller et al., 2021). This difference between the solar wind and

laboratory ion beams makes it difficult to know how to extrapolate from weathering in the laboratory to that in the solar wind.

In addition, experiments commonly form microscopic bubbles or blisters, but these features are generally not found in lunar grains (Keller et al., 2021). The rate at which they form depends on the particle flux (Tamhane and Agrawal, 1979). For example, Matsumoto et al. (2015) found that fluxes of 10^{13} He^+ cm^{-2} s^{-1} created in olivine fully amorphous rims with vesicles and blisters (again, note that olivine does not amorphize in the solar wind). Lower fluxes of 10^{12} He^+ cm^{-2} s^{-1} also fully amorphized a rim, but created only precursors of vesicles, yet even this lower flux is about 4 orders of magnitude higher than that of the solar wind. Similarly, Zhu et al. (2014) irradiated ilmenite with He^+ and found that small flakes formed on the sample. Such flakes are not found on lunar soils, and the authors suggested that the high experimental fluxes caused the difference.

Remote sensing observations of asteroids also reveal a disagreement with solar wind experiments. The timescales needed for irradiation experiments to saturate weathering alterations correspond to $\sim 10^3 - 10^4$ yr of exposure to the solar wind in the inner Solar System (Loeffler et al., 2009; Brunetto et al., 2014). Asteroids appear optically immature, however, and the observed timescale for weathering is $\sim 10^8 - 10^9$ yr (see the review by Shestopalov et al. (2013)). While laser irradiation seems to produce space weathering on timescales similar to what is observed, ion irradiation results in predicted timescales that are orders of magnitude shorter (Willman et al., 2010), again showing that there seems to be a fundamental difference between the experiments and the solar wind.

Finally, high fluxes and fluences of charged particles ($\gtrsim 10^{10}$ particles cm^{-2}) are known to cause dielectric breakdown. All of the experiments in Table 1 use fluences that exceed this threshold by many orders of magnitude, and the fluxes are sufficient to rapidly cause breakdown. This does not mean that they all caused breakdown. A few experimenters mentioned taking steps to

prevent charging (see the discussion in the next section), and it may be that others did the same. Other than these exceptions, however, there is no clear difference between the majority of the experiments in Table 1 and the those that caused breakdown. Thus, it is not possible to rule out that breakdown may have occurred in many of the experiments. This does not mean such experiments are irrelevant; as shown below, they may have useful applications throughout the Solar System.

In conclusion, it is necessary to revisit experiments that simulate space weathering by charged particles. Although the discussion above focused mainly on rocky materials, a flux-dependent process like breakdown can also occur in icy materials. In what follows, I focus on the possibility of breakdown in space weathering experiments, and then analyze the conditions of airless bodies throughout the Solar System to determine where breakdown may be important.

3. Space weathering experiments possibly causing breakdown

Breakdown caused by deep dielectric charging has been studied for decades in the laboratory and in spacecraft, where it is the leading cause of anomalies (Trump and Van de Graaff, 1948; Trump and Wright, 1971; Frederickson et al., 1992; Koons et al., 1999). In all these studies, the primary incident particles have been electrons, and thus the conditions for electron-induced breakdown are well-understood. Experiments, observations, and theory have shown that if $\gtrsim 10^{10}$ electrons cm^{-2} are deposited in a dielectric (i.e., electrical insulator) within that dielectric's discharging timescale (the ratio of the dielectric's electrical permittivity to its electrical conductivity), then that material will likely undergo dielectric breakdown—the explosive creation of electrically conductive channels that rapidly dissipate the charging (e.g., Frederickson et al., 1992; Sørensen et al., 1999; Garrett and Evans, 2001; Green and Frederickson, 2006; NASA, 2017). The conditions for ion-induced breakdown are less studied (e.g., Green and Frederickson, 2006; Green and

Dennison, 2008; Baragiola et al., 2002, 2008; Shi et al., 2010, 2012), but I assume that similar conditions apply.

If the incident flux of charged particles exceeds the breakdown fluence divided by the discharging timescale, then breakdown is likely. For example, if a dielectric has a discharging timescale of 10^3 s, then breakdown can be caused by a charged particle flux $\gtrsim 10^7$ cm^{-2} s^{-1} that is incident for at least 10^3 s. If the flux is lower, then the dielectric will dissipate the charging quickly enough that it will avoid breakdown, even after receiving a fluence of $\sim 10^{10}$ charged particles cm^{-2}.

This condition for dielectric breakdown applies to most solid insulators because it depends on the microscopic—not the macroscopic—properties of dielectrics (Budenstein, 1980; Sørensen et al., 1999). Imperfections, like metallic or gaseous inclusions, voids, cracks, or cusp-like protrusions, all make a material susceptible to dielectric breakdown. These locations enhance the local electric field by up to an order of magnitude (Bahder et al., 1982), and form sites where channels of vaporized material can initiate. The channels ($\lesssim 1$ μm diameter) propagate supersonically during breakdown, mainly along dielectric boundaries (Knaur and Budenstein, 1980; Budenstein, 1980; Andres et al., 2001; Cho et al., 2016). This small-scale but explosive process melts and vaporizes the dielectric (Budenstein, 1980), creating a environment that can, for example, reduce iron to its metallic state (Sheffer, 2007; Pasek et al., 2012).

The condition for breakdown was likely exceeded in many of the experiments in Table 1. As an example, a number of experiments used fluxes of $\sim 10^{13}$ cm^{-2} s^{-1}, enough to cause breakdown in $\sim 10^{-3}$ s. Thus, any material with a discharging timescale $\gtrsim 10^{-3}$ s would be at risk of undergoing breakdown. The discharging timescale is the ratio of the permittivity to the electrical conductivity (e.g., Green and Frederickson, 2006). Assuming a permittivity of $\sim 1 - 10$ times the permittivity of free space, the above fluxes would cause breakdown in materials with electrical conductivi-

ties $\lesssim 10^{-8} - 10^{-7}$ S m^{-1}. Such materials would include most Apollo rocks, which have permittivities in this range (Olhoeft and Strangway, 1975) and conductivities within the range of $\sim 10^{-10} - 10^{-7}$ S m^{-1} at a temperature of 300 K (Carrier et al., 1991).

When exposed to such high fluxes, a material's inherent electrical conductivity is augmented by radiation-induced conductivity, or RIC (Adamec, 1968; Frederickson, 1977); this would decrease the material's discharging timescale. RIC is proportional to the dose rate, i.e., the rate at which energy is deposited per unit mass. It can only be found experimentally, but a reasonable estimate for the coefficient of RIC of a lunar analog is $\sim 10^{-16}$ S m^{-1} (rad s^{-1})$^{-1}$ (Jordan et al., 2019).

Assume a 50 keV proton beam irradiates SiO_2 with a flux of 10^{13} cm^{-2} s^{-1}—reasonable values according to Table 1. The penetration depth of this beam is ~ 400 nm (Berger et al., 2005). Assuming that the SiO_2 has a density of 3 g cm^{-3} and that the energy of the beam is deposited equally throughout the penetration depth, the dose rate is $\sim 10^6$ J kg^{-1} s^{-1}, or $\sim 10^8$ rad s^{-1}. The RIC (the product of the coefficient of RIC and the dose rate) would then be $\sim 10^{-8}$ S m^{-1}. This is within the range of the inherent conductivities for lunar rocks, and thus does not significantly affect the discharging timescales estimated above for lunar and asteroidal analogs (it may be different for other materials, like water ice). Although this result needs to be tested experimentally, this estimate suggests that, unless the dose rate were significantly higher, RIC cannot prevent dielectric breakdown under the typical conditions in space weathering experiments.

Some experimenters attempt to keep the target from charging during ion irradiation by simultaneously irradiating it with low energy (sometimes < 1 eV) electrons (e.g., Hapke, 1973; Dukes et al., 1999; Hapke, 2001; Loeffler et al., 2009; Shusterman et al., 2020). This method assumes that, if a sample is kept electrically neutral, it will not experience significant internal charging. This is true when the penetration depths of the two beams are very similar,

as in the case of low energy electrons and an ion beam of $\sim 1-20$ keV (Cazaux and Lehuede, 1992) ($1-10$ keV protons and alphas (helium nuclei) have ranges of 10s to 100s of nm in SiO_2 (Berger et al., 2005; Brunetto et al., 2014)). The experiments using this method had ion beams in this energy range and thus likely did not cause dielectric breakdown (whether such experiments are therefore valid depends on the factors discussed in §2).

Many other experiments in Table 1 use an ion beam in this energy range, but none mention taking steps to neutralize the target, and experiments using electron beam as the primary form of irradiation also do not describe methods taken to prevent charging (the experiments cited in the previous paragraph are the only ones that mention neutralizing the target). Even assuming all these experiments included such measures, they may not have prevented internal differential charging, that is, internal charging caused by the two charge distributions being separated spatially. A number of experiments in Table 1 use ion energies of 50 keV up to 1 MeV. These ions penetrate SiO_2 to depths of $\sim$400 nm to a few microns (Berger et al., 2005; Brunetto et al., 2014), whereas electrons (< 1 eV) from a flood gun likely have ranges of $\lesssim 1$ nm (e.g., Francis et al., 2011) (Fig. 1). The inherent discharging timescale of most dielectrics cannot neutralize these two layers before breakdown-level fluences are reached. For example, although the sample shown in Fig. 1 is neutral, it can have a internal electric field capable of causing breakdown. This raises a question that needs to be investigated: given typical experimental fluxes, what is the minimum separation for which the electrons become unable to neutralize the ions and prevent breakdown? In addition, how is this separation affected by the fact that particle irradiation can heat the target (e.g, Hapke, 1973), thus significantly decreasing the discharging timescale (note that scanning the incident beam can prevent this heating (Zhu et al., 2014))? It is necessary to answer these questions to ensure that breakdown does not occur in such an experiment.

In conclusion, charged particle experiments face two difficulties. First, it

is not known at what point an ion beam is too energetic, and thus penetrates too deeply, to be neutralized by an electron gun. If the penetration depth of the ion beam is too deep, the low energy electrons may not be able to prevent the internal charging and breakdown. This likely did not affect the fewexperiments that explicitly used neutralization techniques (see above), but it may be a problem for experiments using higher energy beams. Second, most experiments do not include explicit steps to prevent internal charging, despite using fluxes and fluences known to cause significant charging and breakdown. Indeed, some of the experiments in Table 1 were designed to cause breakdown in a range of materials (Campins and Krider, 1989; Lemelle et al., 2003; Baragiola et al., 2008; Shi et al., 2010, 2012; Shusterman et al., 2021), but they did not use conditions—whether beam energy, flux, or fluence—that were different from those used in the other experiments (e.g., compare Baragiola et al. (2005) with Baragiola et al. (2008)). Thus, extreme charging and breakdown remain distinct possibilities in experiments that did not attempt neutralization.

As discussed in the previous section, it is already known that high experimental fluxes cause changes that do not occur in the solar wind. The analysis in this section shows that charged particle experiments also risk causing another unexpected change: dielectric breakdown. Not all these experiments necessarily caused breakdown. One possibility is that the risk of breakdown depends in part on beam energy and that beams of sufficiently low energy can be reflected by strong charging prior to breakdown. The lowest energy particles that caused breakdown were 10 keV electrons and 100 keV Ar^+. It may be that particles with significantly lower energies (e.g., ~ 1 keV electrons or $\sim 1 - 10$ keV ions) cannot cause breakdown. It is critical to determine the combinations of target properties and beam energies, fluxes, and fluences that prevent or cause breakdown. Since few experiments have explored these combinations (e.g., Baragiola et al., 2002; Rau et al., 2020), it is not possible to say which experiments in Table 1 may have caused breakdown. If,

however, researchers wish to simulate types of space weathering that are not related to breakdown, they must first demonstrate that their experiments do *not* create conditions conducive to breakdown.

4. Breakdown in the Solar System

There is a need to investigate the possibilities of charging and breakdown on airless bodies (Baragiola et al., 2002). Thus, even if some of the above experiments did cause dielectric breakdown, this does not make them irrelevant to studying space weathering. A number of airless bodies throughout the Solar System are exposed to conditions conducive to breakdown, and such experiments can help determine whether breakdown contributes to space weathering in these locations.

4.1. Dielectric breakdown on the Moon

Dielectric breakdown has been predicted to be an important weathering process in the top $\sim$1 mm of soil on the Moon, where solar energetic particles (SEPs) can deep dielectrically charge the soil (Lemelle et al., 2003; Jordan et al., 2014, 2015; Jordan et al., 2017, 2019). SEPs are mainly isotropic at the Moon, as shown by observations of SEP protons (Joyce et al., 2013; Jordan et al., 2019) and electrons (Halekas et al., 2009; Dresing et al., 2014). They can thus bombard permanently shadowed regions (PSRs) and the nightside of the Moon.

The Galileo spacecraft experienced dielectric breakdown near Earth (1.2 AU) during a series of large SEP events (Fieseler et al., 2002). Thus, breakdown is possible on the Moon if the discharging timescale of the regolith is sufficiently low. The discharging timescale is the ratio of the dielectric's electrical permittivity to its electrical conductivity, and electrical conductivity decreases with decreasing temperature. As a result, the discharging timescale of soil on the nightside and in PSRs is likely on the order of days and weeks (soil on the dayside is sufficiently warm that its discharging timescale is short enough

to prevent significant charging) (Jordan et al., 2015; Jordan et al., 2019). Assuming that the discharging timescale of the regolith is long enough, then large SEP events ($\gtrsim 10^{10}$ cm^{-2}) can cause breakdown in cold soil, and this may have melted and/or vaporized $\sim 3-10\%$ of impact gardened soil, which is less than but comparable to micrometeoroid impacts (Jordan et al., 2019). This is an ongoing process. Observations with the Cosmic Ray Telescope for the Effects of Radiation, or CRaTER (Spence et al., 2010), onboard the Lunar Reconnaissance Orbiter, or LRO (Tooley et al., 2010), suggest that at least two potentially breakdown-causing SEP events have occurred during LRO's mission (Jordan et al., 2015).

There may be evidence that dielectric breakdown plays an important role in space weathering on the Moon. First, observations with the Lyman Alpha Mapping Project (LAMP) on LRO have shown that the soil in PSRs is more porous than in their surroundings (Gladstone et al., 2012; Byron et al., 2019). Because PSRs are cold throughout the lunar day, they should experience more breakdown weathering than their surroundings. In addition, breakdown should fragment and move grains, which may increase the porosity of the upper ~ 1 mm of regolith, thus helping to explain, at least in part, the increased porosity in the PSRs (Jordan et al., 2015; Jordan et al., 2019; Byron et al., 2019).

Second, the reflectance of the maria increases with increasing latitude. Although this observation has been explained by the fact that the flux of the solar wind decreases towards the poles (Hemingway et al., 2015), a better fit is provided by the combined energy fluxes of dielectric breakdown and micrometeoroid impacts (Jordan, 2021). In addition, this model reasonably explains the observed reflectance values of two prominent lunar swirls (at Reiner Gamma and Mare Ingenii), since their associated magnetic anomalies are likely strong enough to prevent potentially breakdown-causing SEP electrons from reaching the surface in those regions. Further work, particularly in the laboratory, is needed to determine whether breakdown does explain

these observations.

Lemelle et al. (2003) devised another way to test whether breakdown weathering has occurred on the Moon. They argued that if a material is too electrically conductive, or too insulating, then breakdown weathering is less likely. Thus, the test could be similar to that suggested by Taylor et al. (2010), who found that the composition of agglutinitic glasses in lunar soils could be explained by the relative melting temperatures of "glass $>$ plagioclase $>$ pyroxene $\gg$ ilmenite." Could it be that the relative abundances are also related to electrical conductivity, i.e., the more conductive materials are less likely to experience breakdown and be melted? This is one way to test the prediction of Lemelle et al. (2003).

At this point, it appears that some regions on the Moon meet the criteria for breakdown during large SEP events, and there is some evidence that this process plays a role in space weathering. Some of the experiments in Table 1 may be useful in determining whether this is the case. It is important to note, however, that charging on the Moon takes place over $\sim$1 mm, i.e., over many grain diameters (Jordan et al., 2014), whereas in many of the lunar experiments, the charging takes place on sub-grain scales ($\sim$100 nm). Thus, breakdown on the Moon may cause macroscopic changes that do not occur in typical irradiation experiments, and these experiments would need to be modified to further investigate the possibility of breakdown weathering on the Moon.

4.2. Dielectric breakdown on asteroids

In general, asteroids are unlikely to experience significant breakdown weathering. First, the flux of SEP events decreases rapidly with radial distance from the Sun (Lario et al., 2013), so asteroids in the main belt experience much smaller SEP events than does the Moon. In addition, most rotate so fast that night lasts much less than 2 days (Pravec and Harris, 2000) and so is too short for the colder regolith to receive the full fluence of a breakdown-

causing SEP event (Jordan et al., 2019). This is because the high dayside temperatures significantly shorten the discharging timescale (electrical conductivity increases with increasing temperature; see §3 and §4.1). If the discharging timescale of regolith on asteroids is similar to that on the Moon, then any charge built up during the nightside is quickly lost when that region is heated by the Sun (Jordan et al., 2015; Jordan et al., 2019). A given SEP event may have sufficient fluence to cause breakdown, but a region that is heated to daytime temperatures before the event deposits $\sim 10^{10}$ charged particles cm^{-2} will not experience breakdown.

Thus, breakdown-weathered material is not expected in samples from the asteroid 25143 Itokawa or 101955 Bennu. Although both Itokawa are exposed to similar SEP fluxes as the Moon (they have semi-major axes close to 1 AU), they lack the thermal conditions conducive to widespread breakdown weathering. Itokawa rotates about every 12 h (Demura et al., 2006), so its night lasts almost an order of magnitude less than the ~ 2 days needed to receive the full fluence of a breakdown-inducing SEP event (e.g., Jordan et al., 2019). The rotation period of Bennu is about 4 h (Nolan et al., 2013). On these asteroids, breakdown would only occur during the very largest and rarest events, with fluences of $\sim 10^{13}$ cm^{-2} (Jordan et al., 2017).

Despite this, dielectric breakdown may play an important, but more local, role on some asteroids. Depending on SEP fluxes and the exposure time of the soil, breakdown may be significant in permanently shadowed regions, like those on Ceres (Schorghofer et al., 2016), or polar regions that remain in shadow for a significant fraction of the orbit, as on Vesta (Stubbs and Wang, 2012). This contribution to weathering may reveal itself through latitudinal or regional variations in space weathering.

4.3. Dielectric breakdown elsewhere in the Solar System

There are several other locations in the inner Solar System where dielectric breakdown may be important, depending on the discharging timescales

of the soil and its exposure time to SEPs (Fig. 2). First, Mercury is closer to the Sun and so is exposed to higher fluxes of SEPs than is the Moon. Although the planet's magnetic field may reduce the access of SEPs to lower latitudes, SEPs may have access to the cusp regions and to some of the southern hemisphere (Winslow et al., 2014). Breakdown weathering may be important in these locations (Jordan et al., 2014). Second, Phobos and Deimos have high obliquities, causing their polar regions to remain cold for about one-fourth of the martian orbit (~ 0.5 yr). They may thus experience significant breakdown weathering (discussed in detail in Jordan et al. (2018)).

Other experiments in Table 1 deal with comets and the production of OH/H_2O on the Moon. It is beyond the scope of this paper to discuss these in detail, other than to note that these experiments also use fluxes known to cause breakdown. Some bodies in the inner Solar System, like the Moon, do experience such fluxes, so breakdown may play a role in the formation of OH/H_2O on the lunar surface (Huang et al., 2020). Breakdown is likely unimportant on comets: in the inner Solar System, their surfaces are very active, and in the outer Solar System, they likely do not receive sufficient SEP fluxes to undergo breakdown (Lario et al., 2013), although they may experience significant charging by solar UV radiation and the solar wind, leading to the electrostatic levitation of dust (Mendis et al., 1981; Flammer et al., 1986; Mendis and Horányi, 2013; Nordheim et al., 2015). As a result, if any of the experiments focused on comets caused significant charging and/or breakdown, they may not apply as expected.

4.4. Breakdown weathering in Jupiter's magnetosphere

There is, however, one environment in the outer Solar System that is known to cause dielectric breakdown: Jupiter's radiation belts. Eight regular satellites of Jupiter orbit within or near the planet's belts, which form one of the most extreme charged particle environments in the Solar System. Thus,

dielectric breakdown is likely a constant source of space weathering on these satellites. The radiation belts of Uranus and Neptune have much lower fluxes than Earth, whereas Saturn's belts are comparable (Russell and Walker, 1995). Consequently, there is a possibility that breakdown may occur on moons orbiting in Saturn's radiation belts. In this paper, however, I will focus only on the Jovian satellites, since there is both experimental and observational evidence that breakdown is a likely process in this region.

Jupiter's radiation belts are known to cause dielectric breakdown in minutes. Breakdown occurred dozens of times on the Voyager 1 spacecraft as it passed through the radiation belts at distances less than $\sim$12 R_J (Leung et al., 1986). At their peak flux, $\gtrsim$ 1 MeV electrons caused breakdown every ten minutes in electrical insulation inside the spacecraft, consistent with a fluence of $10^{10} - 10^{11}$ electrons cm^{-2} per event (Garrett and Evans, 2001). The Galileo spacecraft also likely experienced internal breakdown events with Jupiter's magnetosphere—always within 30 R_J, and almost always within $\sim$15 R_J (Fieseler et al., 2002).

The surfaces of Jupiter's innermost moons are covered in dielectrics— like sulfur and water ice—that are known to experience breakdown under sufficient fluxes (Campins and Krider, 1989; Baragiola et al., 2008; Shi et al., 2010, 2012). (Note that breakdown in water ice has only been studied with ions, and breakdown in sulfur with electrons.) Furthermore, their surfaces are exposed to the full energy spectrum of charged particles. On Voyager 1, shielding prevented lower energy ($\lesssim$ 1 MeV) electrons from reaching the interior dielectric (cable insulation), thus reducing the rate of charging. The moons, however, are exposed to the full spectrum, and thus much higher fluxes, of charged particles. This should cause breakdown in shorter timescales.

Experiments have shown that breakdown may be important on Io (Campins and Krider, 1989). I will not discuss the moon here, except to point out that these experiments should be revisited to determine if breakdown could create a observable signature. It is uncertain whether other processes, like volcanic

weathering, might hide signs of breakdown.

Instead, I focus first on the three icy Galilean satellites: Europa, Ganymede, and Callisto. They likely have discharging timescales that are $\gtrsim 10^4$ s (Galli et al., 2016). To cause breakdown, a fluence of $\sim 10^{10}$ cm^{-2} must be deposited within that timescale (see §3), corresponding to a flux of $\sim 10^6$ cm^{-2} s^{-1}.

A number of studies have modeled the flux of charged particles as a function of location on these moons. Because they orbit Jupiter at a speed slower than the cold plasma's corotation speed, particles tend to overtake the moons from their trailing hemispheres (electrons drift in the opposite direction, so the situation is reverse for higher energy electrons) (e.g., Paranicas et al., 2007). Each moon absorb the particles as Jupiter's magnetic field lines sweep past, draining the field lines of particles; this means that the flux and energy spectrum of the particles varies as the field lines sweep across the moon. For example, 10 MeV electrons can only impact a small region on the trailing hemisphere of Europa, whereas 100 keV electrons can impact a greater region (Paranicas et al., 2001, 2007), and 10 keV electrons can impact even the leading hemisphere of Europa (Patterson et al., 2012). These complications must be considered when determining whether dielectric breakdown may occur on these moons.

The leading hemisphere of Europa is exposed to lower fluxes of electrons than the trailing hemisphere. As mentioned above, ~ 10 keV electrons can impact anywhere on Europa (Patterson et al., 2012) (note that this energy can cause breakdown, at least in sulfur (Campins and Krider, 1989)). The differential energy flux of $10 - 20$ keV electrons is $\sim 10^{10}$ (cm^2 s sr MeV)$^{-1}$ (see Fig. 3 of Paranicas et al. (2009)). This means that the net energy flux in this energy range is $\sim 10^{10}$ kev cm^{-2} s^{-1}, or $\sim 10^7$ MeV cm^{-2} s^{-1}; indeed, this is approximately the energy flux on the leading hemisphere (see their Fig. 8). Later work, however, suggests that this energy flux may be about an order of magnitude too high (Patterson et al., 2012). Consequently, the number flux of energetic electrons on the leading hemisphere is $\sim 10^8 - 10^9$ cm^{-2} s^{-1}

(cf. Fig. 5 of Paranicas et al. (2009)); the trailing hemisphere, which is exposed to more of the electron energy spectrum, receives a higher flux than this (see also the estimate of Li et al. (2022)). This means that Europa is globally exposed to a flux of electrons that is sufficient to cause breakdown in $\sim 10 - 100$ s.

Although energetic ions do not penetrate as deeply as electrons, their global flux to Europa's surface is $\sim 10^7$ cm^{-2} s^{-1} (Addison et al., 2021), sufficient to cause breakdown in $\sim 10^3$ s—still shorter than the estimated discharging timescale of $\gtrsim 10^4$ s. The fluxes of ions and electrons, then, are sufficient to cause dielectric breakdown across the surface of Europa. This means that it is important to consider not just radiolysis of materials on the surface (e.g., Carlson et al., 2005), but also processing by dielectric breakdown.

The situation is more complex for Ganymede, because it has a magnetic field that affects how charged particles access the surface. Poleward of about $\pm 40°$ latitude, the flux of 4.5 keV to 100 MeV electrons is $\sim 10^8$ cm^{-2} s^{-1} (Liuzzo et al., 2020). At lower latitudes, the flux can be about $6 - 7$ orders of magnitude lower. For energetic ions, the high-latitude flux is $\sim 10^7$ cm^{-2} s^{-1} (?Carnielli et al., 2020), whereas the equatorial regions receive fluxes that are about an order of magnitude lower. According to the results of Carnielli et al. (2020), the low-latitude flux may be $\sim 10^6 - 10^7$ cm^{-2} s^{-1} (see their Fig. 1). Given the discharging timescale assumed above ($\gtrsim 10^4$ s), dielectric breakdown is likely more prevalent at high latitudes (the flux of electrons is much higher here) but could also occur at lower latitudes.

Callisto's trailing, low latitude hemisphere receives a ≤ 30 MeV electron flux of $\sim 10^6$ cm^{-2} s^{-1}, although there are regions in all hemispheres where this full flux can reach the top of the atmosphere (Liuzzo et al., 2019a). The access pattern for ions is different, but the peak flux is $\sim 10^4$ cm^{-2} s^{-1} (Liuzzo et al., 2019b). If electrons alone are needed for breakdown, then it may occur in some regions, but if ions are necessary, then breakdown is

unlikely. In addition, Callisto's atmosphere likely attenuates the flux further, making it unclear whether breakdown is important on Callisto. In addition, most breakdown events on the Voyager 1 and Galileo spacecraft occurred well within Callisto's orbit, suggesting that it is unlikely to occur on the moon (Leung et al., 1986; Fieseler et al., 2002).

Consequently, Europa and the polar regions of Ganymede are the most likely locations on the icy Galilean satellites for dielectric breakdown. The equatorial regions of Ganymede and some locations on Callisto may experience breakdown, perhaps during their night, when the cold temperatures increase the discharging timescales of materials on the surface. The rates of breakdown weathering on Europa and in Ganymede's polar regions would be many orders of magnitude higher than that on the Moon and may create an observational signature. One potential signature may be amorphized ice. Conditions known to cause breakdown also amorphize water ice (e.g., Famá et al. (2010) and references therein). Indeed, some experiments that amorphized water ice with ions were later found also to cause dielectric breakdown (Baragiola et al., 2005, 2008; Shi et al., 2010, 2012). The subsequent condensation of ice vaporized during breakdown would cause it to be amorphous (Hansen and McCord, 2004).

Observations of the satellites seem to be consistent with this prediction. Europa likely experiences breakdown weathering globally, and the top ~ 1 mm of its ice is fully amorphized, beneath which lies crystalline ice (Hansen and McCord, 2004; Ligier et al., 2016). The thickness of this amorphous layer is consistent with the typical penetration depth of the radiation belt particles (Cooper et al., 2001). Ganymede likely experiences a similar rate of breakdown weathering in its high-latitude regions, where the magnetic field lines allow charged particles to reach the surface (Ligier et al., 2019). It may also experience breakdown at lower latitudes, although at lower rates. This is consistent with amorphous ice being found at all latitudes. Finally, Callisto is dominated by crystalline ice, although it may

contain some amorphous ice (Hansen and McCord, 2004). This is consistent with the uncertainty regarding whether Callisto experiences significant breakdown weathering. Thus, dielectric breakdown seems to provide a reasonable explanation for the distribution of amorphous ice on these satellites.

This hypothesis is consistent with where spacecraft have experienced breakdown and with previous work that concluded that the distribution of amorphous ice is governed by the decrease in energetic particle flux from Europa's orbit to Callisto's (Hansen and McCord, 2004; Paranicas et al., 2018). In addition, a simulation was recently developed to predict the expected fraction of water ice that is amorphous on Europa's leading hemisphere, but it was unable to explain the full amount (Berdis et al., 2020). Assuming that the simulation is accurate, it suggests that there may be a missing factor—perhaps breakdown. The relative roles of amorphization by direct irradiation (e.g., Hansen and McCord, 2004; Paranicas et al., 2018) versus that by breakdown should be tested experimentally.

Within the orbits of the Galilean satellites are the four innermost satellites—Adrastea, Metis, Amalthea, and Thebe. In this region, the flux of energetic ions and electrons is even higher. Protons of energies $42 - 131$ MeV have fluxes of at least $\sim 10^7$ cm^{-2} s^{-1} in this region, so the flux of energetic ($\gtrsim 10$ keV) protons must be much higher (Fischer et al., 1996). The flux of ≥ 100 keV electrons is $\sim 10^9$ cm^{-2} s^{-1} (Divine and Garrett, 1983), so the flux of all potentially breakdown-causing electrons ($\gtrsim 10$ keV) is also much higher. These fluxes are sufficient to cause breakdown in $\sim 1 - 100$ s. If so, these moons undergo in seconds the breakdown weathering that Earth's Moon experiences in a year.

No one has yet done a full investigation into the plasma and radiation environments of these satellites, so my discussion will be preliminary. Johnson et al. (2004) suggested that the high fluxes likely darken these moons globally. Given that the conditions for breakdown occur globally on Europa, it seems likely that the same is true for these satellites, which are much

smaller and exposed to higher particle fluxes. The difference between these moons and Europa, however, is that the small moons have very low escapes speeds from their surfaces (no more than tens of m s^{-1}) (Burns et al., 1999, 2004). If breakdown vaporizes water ice on a Galilean surface, the water recondenses on the surface (e.g., Hansen and McCord, 2004). On these small moons, however, breakdown could preferentially remove water ice, leaving a dark lag—perhaps something like spark-created tholins (Sagan and Khare, 1979).

If so, this global darkening might help explain the asymmetrical weathering of the three satellites—Metis, Amalthea, and Thebe—that have been resolved. All have leading hemispheres that are $\sim 25 - 30\%$ brighter than their trailing hemispheres (Thomas et al., 1998; Simonelli et al., 2000). The similarity between all three is surprising, because Metis orbits faster than the cororation speed of the plasma (Adrastea does, as well). The explanation for Europa's asymmetry (e.g., Johnson et al., 1988; Carlson et al., 2005) therefore does not apply to the innermost moons (Thomas et al., 1998).

Meteoroid impacts scour the surfaces of these moons, and the impact flux is highest on the leading hemispheres (e.g., Simonelli et al., 2000). These impacts may scour away the layer of lag on the leading hemispheres quickly enough to counter the darkening caused by breakdown (Simonelli et al., 2000; Johnson et al., 2004). This could explain, for example, why Amalthea appears to made primarily out of water ice (Anderson et al., 2005) but has a trailing edge whose surface material does not seem to be water ice and may contain tholins (Takato et al., 2004). It would also mean that Jupiter's rings, created by this scouring (Ockert-Bell et al., 1999; Burns et al., 1999), are dominated by material that has experienced significant breakdown weathering. These moons could thus provide a way to study the relative roles of impacts and dielectric breakdown in the Jovian system by comparing the scouring rate ($\sim 10^{-5}$ cm yr^{-1} (Burns et al., 1999)) to the expected rate at which breakdown could vaporize water ice.

Consequently, the conditions on seven of the Jovian satellites are conducive to dielectric breakdown, a conclusion supported by experiments and observations of breakdown events on Voyager 1 and Galileo. In addition, breakdown may help explain some puzzling characteristics of these moons. Despite this, few studies have considered the possibility of breakdown, with the exception of Campins and Krider (1989) and Gudipati et al. (2007). Although the above analysis does not prove that dielectric breakdown is a significant process in the Jovian system, it is clear that its likelihood needs to be investigated further, both experimentally and observationally. The experiments of Campins and Krider (1989), Baragiola et al. (2008), and Shi et al. (2010, 2012) need to be revisited to better determine the conditions for and consequences of breakdown on these Jovian moons (e.g., Baragiola et al., 2002).

5. Conclusion

Many experiments have attempted to simulate how charged particles cause space weathering on airless bodies throughout the Solar System (Table 1). Researchers have typically applied these experimental results by assuming that high experimental fluxes cause the same effects as do the significantly lower fluxes found in nature. Recent work, however, has shown that this assumption is not always correct, and high fluxes can alter targets in ways that do not necessarily occur in the Solar System. In particular, high fluxes and fluences of charged particles are known to cause dielectric breakdown. Many of the experiments mentioned above do not describe attempts to prevent the samples from charging. Yet all of the experiments use charged particle fluences $\gtrsim 10^{10}$ cm^{-2}—the threshold for dielectric breakdown in most solid dielectrics. All the experiments in Table 1 exceed this threshold by $4 - 9$ orders of magnitude, and use species and fluxes that are known to cause dielectric breakdown in similar experiments (e.g., Campins and Krider, 1989; Lemelle et al., 2003; Baragiola et al., 2008; Shi et al.,

2010, 2012; Shusterman et al., 2021). Experiments lacking adequate steps to neutralize the target (the exceptions are noted in §3) may cause dielectric breakdown.

This does not mean that such experiments are irrelevant, even if they cause breakdown. I have shown above that a number of locations throughout the Solar System may experience dielectric breakdown, including the Moon and some regions on Mercury, Phobos, Deimos, and some asteroids. In addition, Jupiter's inner satellites may have the highest rates of breakdown weathering in the Solar System. Consequently, it is critical to create experiments to determine the conditions under which dielectric breakdown occurs and the space weathering it causes (Baragiola et al., 2002).

Acknowledgments

This work was supported by NASA grants 80NSSC20M0021 (NASA SSERVI's LEADER) and NNG11PA03C (LRO/CRaTER). The author would like to thank Morgan Shusterman for helpful discussions and Bruce Hapke and an anonymous reviewer for their insightful suggestions.

References

Adamec, V., 1968. Temporary changes in electrical properties of polymer dielectrics due to ionizing radiation. J. Polym. Sci. A2 6, 1241–1253. doi:10.1002/pol.1968.160060704.

Addison, P., Liuzzo, L., Arnold, H., Simon, S., 2021. Influence of Europa's Time Varying Electromagnetic Environment on Magnetospheric Ion Precipitation and Surface Weathering. J. Geophys. Res. 126, e29087. doi:10.1029/2020JA029087.

Anderson, J.D., Johnson, T.V., Schubert, G., Asmar, S., Jacobson, R.A., Johnston, D., Lau, E.L., Lewis, G., Moore, W.B., Taylor, A., Thomas,

P.C., Weinwurm, G., 2005. Amalthea's Density Is Less Than That of Water. Science 308, 1291–1293. doi:10.1126/science.1110422.

Andres, U., Timoshkin, I., Soloviev, M., 2001. Energy consumption and liberation of minerals in explosive electrical breakdown of ores. Miner. Process. Extr. M. 110, 149–157. doi:10.1179/mpm.2001.110.3.149, arXiv:http://www.maneyonline.com/doi/pdf/10.1179/mpm.2001.110.3.149.

Bahder, G., Garrity, T., Sosnowski, M., Eaton, R., Katz, C., 1982. Physical model of electric aging and breakdown of extruded polymeric insulated power cables. IEEE T. Power Ap. and Syst. 6, 1379–1390.

Baragiola, R.A., Atteberry, C.L., Dukes, C.A., Famá, M., Teolis, B.D., 2002. Atomic collisions in solids: Astronomical applications. Nucl. Instrum. Meth. B 193, 720–726. doi:10.1016/S0168-583X(02)00893-5.

Baragiola, R.A., Famá, M., Loeffler, M.J., Raut, U., Shi, J., 2008. Radiation effects in ice: New results. Nuclear Instruments and Methods in Physics Research B 266, 3057–3062. doi:10.1016/j.nimb.2008.03.186.

Baragiola, R.A., Loeffler, M.J., Raut, U., Vidal, R.A., Wilson, C.D., 2005. Laboratory studies of radiation effects in water ice in the outer solar system. Radiation Physics and Chemistry 72, 187–191. doi:10.1016/j.radphyschem.2004.09.013.

Barnett, I.L., Lignell, A., Gudipati, M.S., 2012. Survival Depth of Organics in Ices under Low-energy Electron Radiation (¡=2 keV). Astrophys. J. 747, 13. doi:10.1088/0004-637X/747/1/13.

Behr, P.R., Tribbett, P.D., Robinson, T.D., Loeffler, M.J., 2020. Compaction of Porous H_2O Ice via Energetic Electrons. Astrophys. J. 900, 147. doi:10.3847/1538-4357/abad3f.

Berdis, J.R., Gudipati, M.S., Murphy, J.R., Chanover, N.J., 2020. Europa's surface water ice crystallinity: Discrepancy between observations

and thermophysical and particle flux modeling. Icarus 341, 113660. doi:10.1016/j.icarus.2020.113660, arXiv:2002.04132.

Berger, M.J., Coursey, J.S., Zucker, M.A., Chang, J., 2005. ESTAR, PSTAR, and ASTAR: Computer Programs for Calculating Stopping-Power and Range Tables for Electrons, Protons, and Helium Ions (version 1.2.3). National Institute of Standards and Technology. URL: http://physics.nist.gov/Star. [Online; accessed 29 August 2012].

Bibring, J.P., Borg, J., Burlingame, A.L., Langevin, Y., Maurette, M., Vassent, B., 1975. Solar-wind and solar-flare maturation of the lunar regolith. Lunar and Planetary Science Conference Proceedings 3, 3471–3493.

Bradley, J.P., Ishii, H.A., Gillis-Davis, J.J., Ciston, J., Nielsen, M.H., Bechtel, H.A., Martin, M.C., 2014. Detection of solar wind-produced water in irradiated rims on silicate minerals. Proceedings of the National Academy of Science 111, 1732–1735. doi:10.1073/pnas.1320115111.

Brunetto, R., Lantz, C., Ledu, D., Baklouti, D., Barucci, M.A., Beck, P., Delauche, L., Dionnet, Z., Dumas, P., Duprat, J., Engrand, C., Jamme, F., Oudayer, P., Quirico, E., Sandt, C., Dartois, E., 2014. Ion irradiation of Allende meteorite probed by visible, IR, and Raman spectroscopies. Icarus 237, 278–292. doi:10.1016/j.icarus.2014.04.047.

Budenstein, P.P., 1980. On the mechanism of dielectric breakdown of solids. IEEE T. Electr. Insul. 3, 225–240.

Burns, J.A., Showalter, M.R., Hamilton, D.P., Nicholson, P.D., de Pater, I., Ockert-Bell, M.E., Thomas, P.C., 1999. The Formation of Jupiter's Faint Rings. Science 284, 1146. doi:10.1126/science.284.5417.1146.

Burns, J.A., Simonelli, D.P., Showalter, M.R., Hamilton, D.P., Porco, C.D., Throop, H., Esposito, L.W., 2004. Jupiter's ring-moon system, in: Bagenal, Fran and Dowling, Timothy E. and McKinnon, William B. (Ed.),

Jupiter. The Planet, Satellites and Magnetosphere. Cambridge Univ.. volume 1, pp. 241–262.

Byron, B.D., Retherford, K.D., Greathouse, T.K., Mand t, K.E., Hendrix, A.R., Poston, M.J., Liu, Y., Cahill, J.T., Mazarico, E., 2019. Effects of Space Weathering and Porosity on the Far-UV Reflectance of Amundsen Crater. J. Geophys. Res. Planets 124, 823–836. doi:10.1029/2018JE005908.

Campins, H., Krider, E.P., 1989. Surface discharges on natural dielectrics in the solar system. Science 245, 622–624. doi:10.1126/science.245.4918.622.

Carlson, R.W., Anderson, M.S., Mehlman, R., Johnson, R.E., 2005. Distribution of hydrate on Europa: Further evidence for sulfuric acid hydrate. Icarus 177, 461–471. doi:10.1016/j.icarus.2005.03.026.

Carnielli, G., Galand, M., Leblanc, F., Modolo, R., Beth, A., Jia, X., 2020. Simulations of ion sputtering at Ganymede. Icarus 351, 113918. doi:10.1016/j.icarus.2020.113918.

Carrez, P., Demyk, K., Cordier, P., Gengembre, L., Grimblot, J., D'Hendecourt, L., Jones, A.P., Leroux, H., 2002. Low-energy helium ion irradiation-induced amorphization and chemical changes in olivine: Insights for silicate dust evolution in the interstellar medium. Meteorit. Planet. Sci. 37, 1599–1614. doi:10.1111/j.1945-5100.2002.tb00814.x.

Carrier, III, W.D., Olhoeft, G.R., Mendell, W., 1991. Physical properties of the lunar surface, in: Heiken, G., and Vaniman, D., and French, B. M. (Ed.), Lunar Sourcebook. Cambridge Univ., Cambridge, pp. 475–594.

Cassidy, W., Hapke, B., 1975. Effects of Darkening Processes on Surfaces of Airless Bodies. Icarus 25, 371–383. doi:10.1016/0019-1035(75)90002-0.

Cazaux, J., Lehuede, P., 1992. Some physical descriptions of the charging effects of insulators under incident particle bombardment. J. Electron Spectrosc. 59, 49–71.

Cho, S.H., Cheong, S.S., Yokota, M., Kaneko, K., 2016. The Dynamic Fracture Process in Rocks Under High-Voltage Pulse Fragmentation. Rock Mechanics and Rock Engineering 49, 3841–3853. doi:10.1007/s00603-016-1031-z.

Christoffersen, R., Keller, L.P., 2007. Space Plasma Ion Processing of Ilmenite in the Lunar Soil: Insights from In-Situ TEM Ion Irradiation Experiments, in: Lunar and Planetary Science Conference, p. 1969.

Christoffersen, R., Keller, L.P., Dukes, C., 2020. The Role of Solar Wind Ion Processing in Space Weathering of Olivine: Unraveling the Paradox of Laboratory Irradiation Results Compared to Observations of Natural Samples, in: Lunar and Planetary Science Conference, p. 2147.

Cooper, J.F., Johnson, R.E., Mauk, B.H., Garrett, H.B., Gehrels, N., 2001. Energetic Ion and Electron Irradiation of the Icy Galilean Satellites. Icarus 149, 133–159. doi:10.1006/icar.2000.6498.

Demura, H., Kobayashi, S., Nemoto, E., Matsumoto, N., Furuya, M., Yukishita, A., Muranaka, N., Morita, H., Shirakawa, K., Maruya, M., Ohyama, H., Uo, M., Kubota, T., Hashimoto, T., Kawaguchi, J., Fujiwara, A., Saito, J., Sasaki, S., Miyamoto, H., Hirata, N., 2006. Pole and Global Shape of 25143 Itokawa. Science 312, 1347–1349. doi:10.1126/science.1126574.

Divine, N., Garrett, H.B., 1983. Charged particle distributions in Jupiter's magnetosphere. J. Geophys. Res. 88, 6889–6903. doi:10.1029/JA088iA09p06889.

Dresing, N., Gómez-Herrero, R., Heber, B., Klassen, A., Malandraki, O., Dröge, W., Kartavykh, Y., 2014. Statistical survey of widely spread out solar electron events observed with STEREO and ACE with special attention to anisotropies. Astron. Astrophys. 567, A27. doi:10.1051/0004-6361/201423789.

Dukes, C.A., Baragiola, R.A., McFadden, L.A., 1999. Surface modification of olivine by H^+ and He^+ bombardment. J. Geophys. Res. 104, 1865–1872. doi:10.1029/98JE02820.

Famá, M., Loeffler, M.J., Raut, U., Baragiola, R.A., 2010. Radiation-induced amorphization of crystalline ice. Icarus 207, 314–319. doi:10.1016/j.icarus.2009.11.001.

Fieseler, P.D., Ardalan, S.M., Frederickson, A.R., 2002. The radiation effects on galileo spacecraft systems at jupiter. IEEE Trans. Nucl. Sci. 49, 2739–2758. doi:10.1109/TNS.2002.805386.

Fischer, H.M., Pehlke, E., Wibberenz, G., Lanzerotti, L.J., Mihalov, J.D., 1996. High-Energy Charged Particles in the Innermost Jovian Magnetosphere. Science 272, 856–858. doi:10.1126/science.272.5263.856.

Flammer, K.R., Jackson, B., Mendis, D.A., 1986. On the Brightness Variations of Comet Halley at Large Heliocentric Distances. Earth Moon and Planets 35, 203–212. doi:10.1007/BF00058065.

Francis, Z., Incerti, S., Karamitros, M., Tran, H.N., Villagrasa, C., 2011. Stopping power and ranges of electrons, protons and alpha particles in liquid water using the Geant4-DNA package. Nucl. Instrum. Meth. B 269, 2307–2311. doi:10.1016/j.nimb.2011.02.031.

Frederickson, A.R., 1977. Radiation Induced Currents and Conductivity in Dielectrics. IEEE T. Nucl. Sci. 24, 2532–2539. doi:10.1109/TNS.1977.4329251.

Frederickson, A.R., Holeman, E.G., Mullen, E.G., 1992. Characteristics of spontaneous electrical discharging of various insulators in space radiations. IEEE T. Nucl. Sci. 39, 1773–1782. doi:10.1109/23.211366.

Fu, X., Zou, Y., Zheng, Y., Ouyang, Z., 2012. Effects of space weathering

on diagnostic spectral features: Results from He^+ irradiation experiments. Icarus 219, 630–640. doi:10.1016/j.icarus.2012.03.009.

Galli, A., Vorburger, A., Pommerol, A., Wurz, P., Jost, B., Poch, O., Brouet, Y., Tulej, M., Thomas, N., 2016. Surface charging of thick porous water ice layers relevant for ion sputtering experiments. Planet. Space Sci. 126, 63–71. doi:10.1016/j.pss.2016.03.016, arXiv:1701.04204.

Garrett, H.B., Evans, R.W., 2001. Internal Electrostatic Discharge Environment at Jupiter, in: Harris, R.A. (Ed.), Spacecraft Charging Technology, pp. 609–619.

Gladstone, G.R., Retherford, K.D., Egan, A.F., Kaufmann, D.E., Miles, P.F., Parker, J.W., Horvath, D., Rojas, P.M., Versteeg, M.H., Davis, M.W., Greathouse, T.K., Slater, D.C., Mukherjee, J., Steffl, A.J., Feldman, P.D., Hurley, D.M., Pryor, W.R., Hendrix, A.R., Mazarico, E., Stern, S.A., 2012. Far-ultraviolet reflectance properties of the Moon's permanently shadowed regions. J. Geophys. Res. Planet 117, E00H04. doi:10.1029/2011JE003913.

Green, N.W., Dennison, J.R., 2008. Deep Dielectric Charging of Spacecraft Polymers by Energetic Protons. IEEE T. Plasma Sci. 36, 2482–2490. doi:10.1109/TPS.2008.2003442.

Green, N.W., Frederickson, A.R., 2006. A Study of Spacecraft Charging Due to Exposure to Interplanetary Protons, in: El-Genk, M.S. (Ed.), Space Technology and Applications International Forum - STAIF 2006, pp. 694–700. doi:10.1063/1.2169250.

Gudipati, M.S., Allamandola, L.J., Cooper, J.F., Sturner, S.J., Johnson, R.E., 2007. Consequence of Electron Mobility in Icy Grains on Solar System Objects, in: AGU Fall Meeting Abstracts, pp. P53B–1248.

Halekas, J.S., Delory, G.T., Lin, R.P., Stubbs, T.J., Farrell, W.M., 2009.

Lunar surface charging during solar energetic particle events: Measurement and prediction. J. Geophys. Res. 114, 5110. doi:10.1029/2009JA014113.

Hansen, G.B., McCord, T.B., 2004. Amorphous and crystalline ice on the Galilean satellites: A balance between thermal and radiolytic processes. J. Geophys. Res. Planets 109, E01012. doi:10.1029/2003JE002149.

Hapke, B., 1965. Effects of a Simulated Solar Wind on the Photometric Properties of Rocks and Powders. Annals of the New York Academy of Sciences 123, 711–721. doi:10.1111/j.1749-6632.1965.tb20395.x.

Hapke, B., 1968. Lunar Surface: Composition Inferred from Optical Properties. Science 159, 76–79. doi:10.1126/science.159.3810.76.

Hapke, B., 1973. Darkening of Silicate Rock Powders by Solar Wind Sputtering. Moon 7, 342–355. doi:10.1007/BF00564639.

Hapke, B., 2001. Space weathering from Mercury to the asteroid belt. J. Geophys. Res. 106, 10,039–10,074. doi:10.1029/2000JE001338.

Hapke, B., Cassidy, W., Wells, E., 1975. Effects of vapor-phase deposition processes on the optical, chemical, and magnetic properties of the lunar regolith. Moon 13, 339–353. doi:10.1007/BF00567525.

Hapke, B.W., Cohen, A.J., Cassidy, W.A., Wells, E.N., 1970. Solar radiation effects on the optical properties of Apollo 11 samples. Geochimica et Cosmochimica Acta Supplement 1, 2199.

Heide, H.G., 1984. Observations on ice layers. Ultramicroscopy 14, 271–278.

Hemingway, D.J., Garrick-Bethell, I., Kreslavsky, M.A., 2015. Latitudinal variation in spectral properties of the lunar maria and implications for space weathering. Icarus 261, 66–79. doi:10.1016/j.icarus.2015.08.004.

Henderson, B.L., Gudipati, M.S., Bateman, F.B., 2019. Leeb hardness of salty Europa ice analogs exposed to high-energy electrons. Icarus 322, 114–120. doi:10.1016/j.icarus.2019.01.006.

Huang, Z., Nomuroa, K., Wang, J., 2020. The Role of Dielectric Breakdown in the Formation of Water Molecules in Lunar Regolith, in: Lunar and Planetary Science Conference, p. 2692.

Ichimura, A.S., Zent, A.P., Quinn, R.C., Sanchez, M.R., Taylor, L.A., 2012. Hydroxyl (OH) production on airless planetary bodies: Evidence from H^+/D^+ ion-beam experiments. Earth and Planetary Science Letters 345, 90–94. doi:10.1016/j.epsl.2012.06.027.

Johnson, R.E., Carlson, R.W., Cooper, J.F., Paranicas, C., Moore, M.H., Wong, M.C., 2004. Radiation effects on the surfaces of the Galilean satellites, in: Bagenal, F., Dowling, T.E., McKinnon, W.B. (Eds.), Jupiter. The Planet, Satellites and Magnetosphere. volume 1, pp. 485–512.

Johnson, R.E., Nelson, M.L., Nccord, T.B., Gradie, J.C., 1988. Analysis of Voyager images of Europa: Plasma bombardment. Icarus 75, 423–436. doi:10.1016/0019-1035(88)90155-8.

Jordan, A.P., 2021. Evidence for dielectric breakdown weathering on the Moon. Icarus 358, 114199. doi:10.1016/j.icarus.2020.114199.

Jordan, A.P., Stubbs, T.J., Shusterman, M.L., Izenberg, N.R., Wilson, J.K., Hayne, P.O., Schwadron, N.A., Spence, H.E., 2019. How dielectric breakdown may contribute to the global weathering of regolith on the Moon. Icarus 319, 785–794. doi:10.1016/j.icarus.2018.10.025.

Jordan, A.P., Stubbs, T.J., Wilson, J.K., Schwadron, N.A., Spence, H.E., 2015. Dielectric breakdown weathering of the moon's polar regolith. J. Geophys. Res. Planets 120, 210–225. doi:10.1002/2014JE004710.

Jordan, A.P., Stubbs, T.J., Wilson, J.K., Schwadron, N.A., Spence, H.E., 2017. The rate of dielectric breakdown weathering of lunar regolith in permanently shadowed regions. Icarus 283, 352–358. doi:10.1016/j.icarus.2016.08.027.

Jordan, A.P., Stubbs, T.J., Wilson, J.K., Schwadron, N.A., Spence, H.E., 2018. The possible contribution of dielectric breakdown to space weathering on Phobos. Advances in Space Research 62, 2187–2198. doi:10.1016/j.asr.2018.01.029.

Jordan, A.P., Stubbs, T.J., Wilson, J.K., Schwadron, N.A., Spence, H.E., Joyce, C.J., 2014. Deep dielectric charging of regolith within the moon's permanently shadowed regions. J. Geophys. Res. Planets 119, 1806–1821. doi:10.1002/2014JE004648.

Joyce, C.J., Schwadron, N.A., Wilson, J.K., Spence, H.E., Kasper, J.C., Golightly, M., Blake, J.B., Mazur, J., Townsend, L.W., Case, A.W., Semones, E., Smith, S., Zeitlin, C.J., 2013. Validation of PREDICCS using LRO/CRaTER observations during three major solar events in 2012. Space Weather 11, 350–360. doi:10.1002/swe.20059.

Kanuchova, Z., Brunetto, R., Fulvio, D., Strazzulla, G., 2015. Near-ultraviolet bluing after space weathering of silicates and meteorites. Icarus 258, 289–296. doi:10.1016/j.icarus.2015.06.030.

Keller, L.P., Berger, E.L., Zhang, S., Christoffersen, R., 2021. Solar energetic particle tracks in lunar samples: A transmission electron microscope calibration and implications for lunar space weathering. Meteorit. Planet. Sci. , 1685–1707doi:10.1111/maps.13732.

Keller, L.P., McKay, D.S., 1997. The nature and origin of rims on lunar soil grains. Geochim. Cosmochim. Ac. 61, 2331–2341. doi:10.1016/S0016-7037(97)00085-9.

Knaur, J.A., Budenstein, P.P., 1980. Impulse breakdown in pmma under megavolt, nanosecond excitation. IEEE T. Electr. Insul. EI-15, 313–321. doi:10.1109/TEI.1980.298257.

Koons, H.C., Mazur, J.E., Selesnick, R.S., Blake, J.B., Fennell, J.F., 1999. The impact of the space environment on space systems. NASA STI/Recon Technical Report N , 7–11.

Lantz, C., Brunetto, R., Barucci, M.A., Dartois, E., Duprat, J., Engrand, C., Godard, M., Ledu, D., Quirico, E., 2015. Ion irradiation of the Murchison meteorite: Visible to mid-infrared spectroscopic results. Astron. Astrophys. 577, A41. doi:10.1051/0004-6361/201425398.

Lantz, C., Brunetto, R., Barucci, M.A., Fornasier, S., Baklouti, D., Bourçois, J., Godard, M., 2017. Ion irradiation of carbonaceous chondrites: A new view of space weathering on primitive asteroids. Icarus 285, 43–57. doi:10.1016/j.icarus.2016.12.019.

Lario, D., Aran, A., Gómez-Herrero, R., Dresing, N., Heber, B., Ho, G.C., Decker, R.B., Roelof, E.C., 2013. Longitudinal and Radial Dependence of Solar Energetic Particle Peak Intensities: STEREO, ACE, SOHO, GOES, and MESSENGER Observations. Astrophys. J. 767, 41. doi:10.1088/0004-637X/767/1/41.

Lemelle, L., Beaunier, L., Borensztajn, S., Fialin, M., Guyot, F., 2003. Destabilization of olivine by 30-keV electron irradiation: a possible mechanism of space weathering affecting interplanetary dust particles and planetary surfaces. Geochim. Cosmochim. Ac. 67, 1901–1910. doi:10.1016/S0016-7037(02)01273-5.

Lepault, J., Freeman, R., Dubochet, J., 1983. Electron beam induced "vitrified ice". J. Microscopy 132, RP3–RP4.

Leung, P., Whittlesey, A.C., Garrett, H.B., Robinson, Jr., P.A., 1986. Environment-Induced Electrostatic Discharges as the Cause of Voyager 1 Power-On Resets. J. Spacecraft Rockets 23, 323–330. doi:10.2514/3.25805.

Li, J., Gudipati, M.S., Mishra, Y.N., Liang, M.C., Yung, Y.L., 2022. Oxidant generation in the ice under electron irradiation: Simulation and application to Europa. Icarus 373, 114760. doi:10.1016/j.icarus.2021.114760.

Ligier, N., Paranicas, C., Carter, J., Poulet, F., Calvin, W.M., Nordheim, T.A., Snodgrass, C., Ferellec, L., 2019. Surface composition and properties of Ganymede: Updates from ground-based observations with the near-infrared imaging spectrometer SINFONI/VLT/ESO. Icarus 333, 496–515. doi:10.1016/j.icarus.2019.06.013, arXiv:1910.07445.

Ligier, N., Poulet, F., Carter, J., Brunetto, R., Gourgeot, F., 2016. VLT/SINFONI Observations of Europa: New Insights into the Surface Composition. Astrophys. J. 151, 163. doi:10.3847/0004-6256/151/6/163.

Liuzzo, L., Poppe, A.R., Paranicas, C., Nénon, Q., Fatemi, S., Simon, S., 2020. Variability in the Energetic Electron Bombardment of Ganymede. J. Geophys. Res. 125, e28347. doi:10.1029/2020JA028347.

Liuzzo, L., Simon, S., Regoli, L., 2019a. Energetic electron dynamics near Callisto. Planet. Space Sci. 179, 104726. doi:10.1016/j.pss.2019.104726.

Liuzzo, L., Simon, S., Regoli, L., 2019b. Energetic ion dynamics near Callisto. Planet. Space Sci. 166, 23–53. doi:10.1016/j.pss.2018.07.014.

Loeffler, M.J., Dukes, C.A., Baragiola, R.A., 2009. Irradiation of olivine by 4 keV He^+: Simulation of space weathering by the solar wind. J. Geophys. Res. Planets 114, E03003. doi:10.1029/2008JE003249.

Loeffler, M.J., Tribbett, P.D., Cooper, J.F., Sturner, S.J., 2020. A possible explanation for the presence of crystalline H_2O-ice on Kuiper Belt Objects. Icarus 351, 113943. doi:10.1016/j.icarus.2020.113943.

Managadze, G.G., Cherepin, V.T., Shkuratov, Y.G., Kolesnik, V.N., Chumikov, A.E., 2011. Simulating OH/H $_2$O formation by solar wind at the lunar surface. Icarus 215, 449–451. doi:10.1016/j.icarus.2011.06.025.

Matsumoto, T., Tsuchiyama, A., Watanabe, N., Yasuda, K., Miyake, A., Nakauchi, Y., Okada, T., Abe, M., Yada, T., Uesugi, M., Karouji, Y., Nakato, A., Hashiguschi, M., Kumagai, K., 2015. Systematic Ion Irradiation Experiments to Olivine: Comparison with Space Weathered Rims of Itokawa Regolith Particles, in: Space Weathering of Airless Bodies: An Integration of Remote Sensing Data, Laboratory Experiments and Sample Analysis Workshop, p. 2045.

Meier, R.M., Loeffler, M.J., 2020. Sputtering of water ice by keV electrons at 60 K. Surface Sci. 691, 121509. doi:10.1016/j.susc.2019.121509.

Mendis, D.A., Hill, J.R., Houpis, H.L.F., Whipple, E.C., 1981. On the electrostatic charging of the cometary nucleus. Astrophys. J. 249, 787–797. doi:10.1086/159337.

Mendis, D.A., Horányi, M., 2013. Dusty Plasma Effects in Comets: Expectations for Rosetta. Rev. Geophys. 51, 53–75. doi:10.1002/rog.20005.

NASA, 2017. Mitigating In-Space Charging Effects—A Guideline. Technical Report. NASA-HDBK-4002A. Washington, DC.

Nolan, M.C., Magri, C., Howell, E.S., Benner, L.A.M., Giorgini, J.D., Hergenrother, C.W., Hudson, R.S., Lauretta, D.S., Margot, J.L., Ostro, S.J., Scheeres, D.J., 2013. Shape model and surface properties of the OSIRIS-REx target Asteroid (101955) Bennu from radar and lightcurve observations. Icarus 226, 629–640. doi:10.1016/j.icarus.2013.05.028.

Nordheim, T.A., Jones, G.H., Halekas, J.S., Roussos, E., Coates, A.J., 2015. Surface charging and electrostatic dust acceleration at the nucleus

of comet 67P during periods of low activity. Planet. Space Sci. 119, 24–35. doi:10.1016/j.pss.2015.08.008.

Ockert-Bell, M.E., Burns, J.A., Daubar, I.J., Thomas, P.C., Veverka, J., Belton, M.J.S., Klaasen, K.P., 1999. The Structure of Jupiter's Ring System as Revealed by the Galileo Imaging Experiment. Icarus 138, 188–213. doi:10.1006/icar.1998.6072.

Olhoeft, G.R., Strangway, D.W., 1975. Dielectric properties of the first 100 meters of the moon. Earth Planet. Sc. Lett. 24, 394–404. doi:10.1016/0012-821X(75)90146-6.

Paranicas, C., Carlson, R.W., Johnson, R.E., 2001. Electron bombardment of Europa. Geophys. Res. Lett. 28, 673–676. doi:10.1029/2000GL012320.

Paranicas, C., Cooper, J.F., Garrett, H.B., Johnson, R.E., Sturner, S.J., 2009. Europa's Radiation Environment and Its Effects on the Surface, in: Pappalardo, R.T., McKinnon, W.B., Khurana, K.K. (Eds.), Europa. Univ. Arizona, p. 529.

Paranicas, C., Hibbitts, C.A., Kollmann, P., Ligier, N., Hendrix, A.R., Nordheim, T.A., Roussos, E., Krupp, N., Blaney, D., Cassidy, T.A., Clark, G., 2018. Magnetospheric considerations for solar system ice state. Icarus 302, 560–564. doi:10.1016/j.icarus.2017.12.013.

Paranicas, C., Mauk, B.H., Khurana, K., Jun, I., Garrett, H., Krupp, N., Roussos, E., 2007. Europa's near-surface radiation environment. Geophys. Res. Lett. 34, L15103. doi:10.1029/2007GL030834.

Pasek, M.A., Block, K., Pasek, V., 2012. Fulgurite morphology: a classification scheme and clues to formation. Contrib. Mineral. Petr. 164, 477–492. doi:10.1007/s00410-012-0753-5.

Patterson, G.W., Paranicas, C., Prockter, L.M., 2012. Characterizing electron bombardment of Europa's surface by location and depth. Icarus 220, 286–290. doi:10.1016/j.icarus.2012.04.024.

Pieters, C.M., Noble, S.K., 2016. Space weathering on airless bodies. J. Geophys. Res. Planets 121, 1865–1884. doi:10.1002/2016JE005128. 2016JE005128.

Poppe, A.R., Farrell, W.M., Halekas, J.S., 2018. Formation Timescales of Amorphous Rims on Lunar Grains Derived From ARTEMIS Observations. J. Geophys. Res. Planets 123, 37–46. doi:10.1002/2017JE005426.

Pravec, P., Harris, A.W., 2000. Fast and Slow Rotation of Asteroids. Icarus 148, 12–20. doi:10.1006/icar.2000.6482.

Rau, E.I., Tatarintsev, A.A., Zykova, E.Y., Markovets (Ozerova), K.E., Minnebaev, K.F., 2020. Charging of dielectrics under ion irradiation. Vacuum 177, 109373. doi:10.1016/j.vacuum.2020.109373.

Russell, C.T., Walker, R.J., 1995. The magnetospheres of the outer planets, in: Kivelson, M.G., Russell, C.T. (Eds.), Introduction to Space Physics. Cambridge Univ.. volume 1, pp. 503–520.

Sagan, C., Khare, B.N., 1979. Tholins: organic chemistry of interstellar grains and gas. Nature 277, 102–107. doi:10.1038/277102a0.

Schorghofer, N., Mazarico, E., Platz, T., Preusker, F., Schröder, S.E., Raymond, C.A., Russell, C.T., 2016. The permanently shadowed regions of dwarf planet Ceres. Geophys. Res. Lett. 43, 6783–6789. doi:10.1002/2016GL069368.

Sheffer, A.A., 2007. Chemical Reduction of Silicates by Meteorite Impacts and Lightning Strikes. Ph.D. thesis. University of Arizona.

Shestopalov, D.I., Golubeva, L.F., Cloutis, E.A., 2013. Optical maturation of asteroid surfaces. Icarus 225, 781–793. doi:10.1016/j.icarus.2013.05.002.

Shi, J., Famá, M., Teolis, B.D., Baragiola, R.A., 2010. Ion-induced electrostatic charging of ice. Nucl. Instrum. Meth. B 268, 2888–2891. doi:10.1016/j.nimb.2010.04.013.

Shi, J., Famá, M., Teolis, B.D., Baragiola, R.A., 2012. Ion-induced electrostatic charging of ice at 15-160 K. Phys. Rev. B 85, 035424. doi:10.1103/PhysRevB.85.035424.

Shusterman, M.L., Sharp, T.G., Robinson, M.S., 2021. Dielectric breakdown weathering: Morphological effects of electrical breakdown in laboratory-irradiated San Carlos olivine, in: Lunar and Planetary Science Conference, p. 2141.

Shusterman, M.L., Sharp, T.G., Robinson, M.S., Rahman, Z., Keller, L.P., Dukes, C.A., Bu, C., Roldan, M.A., 2020. The Role of Solar Wind Hydrogen in Space Weathering: Insights from Laboratory-Irradiated Northwest Africa 12008, in: 51st Lunar and Planetary Science Conference, p. 2704.

Simonelli, D.P., Rossier, L., Thomas, P.C., Veverka, J., Burns, J.A., Belton, M.J.S., 2000. Leading/Trailing Albedo Asymmetries of Thebe, Amalthea, and Metis. Icarus 147, 353–365. doi:10.1006/icar.2000.6474.

Sørensen, J., Rodgers, D., Ryden, K., Latham, P., Wrenn, G., Levy, L., Panabiere, G., 1999. Esa's tools for internal charging, in: 5th European Conference on Radiation and Its Effects on Components and Systems (RADECS), 1999, pp. 27 –33. doi:10.1109/RADECS.1999.858540.

Spence, H.E., Case, A.W., Golightly, M.J., Heine, T., Larsen, B.A., Blake, J.B., Caranza, P., Crain, W.R., George, J., Lalic, M., Lin, A., Looper, M.D., Mazur, J.E., Salvaggio, D., Kasper, J.C., Stubbs, T.J., Doucette, M., Ford, P., Foster, R., Goeke, R., Gordon, D., Klatt, B., O'Connor,

J., Smith, M., Onsager, T., Zeitlin, C., Townsend, L.W., Charara, Y., 2010. CRaTER: The Cosmic Ray Telescope for the Effects of Radiation Experiment on the Lunar Reconnaissance Orbiter Mission. Space Sci. Rev. 150, 243–284. doi:10.1007/s11214-009-9584-8.

Strazzulla, G., Baratta, G.A., Johnson, R.E., Donn, B., 1991. Primordial comet mantle: Irradiation production of a stable organic crust. Icarus 91, 101–104. doi:10.1016/0019-1035(91)90129-H.

Stubbs, T.J., Wang, Y., 2012. Illumination conditions at the Asteroid 4 Vesta: Implications for the presence of water ice. Icarus 217, 272–276. doi:10.1016/j.icarus.2011.11.007.

Takato, N., Bus, S.J., Terada, H., Pyo, T.S., Kobayashi, N., 2004. Detection of a Deep 3-μm Absorption Feature in the Spectrum of Amalthea (JV). Science 306, 2224–2227. doi:10.1126/science.1105427.

Tamhane, A.S., Agrawal, J.K., 1979. Diffusion of rare gases of solar wind origin from lunar fines as bubbles. Earth Planet. Sci. Lett. 42, 243–250. doi:10.1016/0012-821X(79)90031-1.

Taylor, L.A., Pieters, C., Patchen, A., Taylor, D.H.S., Morris, R.V., Keller, L.P., McKay, D.S., 2010. Mineralogical and chemical characterization of lunar highland soils: Insights into the space weathering of soils on airless bodies. J. Geophys. Res. Planets 115, E02002. doi:10.1029/2009JE003427.

Thomas, P.C., Burns, J.A., Rossier, L., Simonelli, D., Veverka, J., Chapman, C.R., Klaasen, K., Johnson, T.V., Belton, M.J.S., Galileo Solid State Imaging Team, 1998. The Small Inner Satellites of Jupiter. Icarus 135, 360–371. doi:10.1006/icar.1998.5976.

Tooley, C.R., Houghton, M.B., Saylor, R.S., Peddie, C., Everett, D.F., Baker, C.L., Safdie, K.N., 2010. Lunar Reconnaissance Orbiter Mission

and Spacecraft Design. Space Sci. Rev. 150, 23–62. doi:10.1007/s11214-009-9624-4.

Trump, J.G., Van de Graaff, R.J., 1948. Irradiation of biological materials by high energy roentgen rays and cathode rays. J. Appl. Phys. 19, 599–604. doi:10.1063/1.1698178.

Trump, J.G., Wright, K.A., 1971. Injection of megavolt electrons into solid dielectrics. Mater. Res. Bull. 6, 1075–1083. doi:10.1016/0025-5408(71)90087-0.

Willman, M., Jedicke, R., Moskovitz, N., Nesvorný, D., Vokrouhlický, D., Mothé-Diniz, T., 2010. Using the youngest asteroid clusters to constrain the space weathering and gardening rate on S-complex asteroids. Icarus 208, 758–772. doi:10.1016/j.icarus.2010.02.017, arXiv:1004.3823.

Winslow, R.M., Johnson, C.L., Anderson, B.J., Gershman, D.J., Raines, J.M., Lillis, R.J., Korth, H., Slavin, J.A., Solomon, S.C., Zurbuchen, T.H., Zuber, M.T., 2014. Mercury's surface magnetic field determined from proton-reflection magnetometry. Geophys. Res. Lett. 41, 4463–4470. doi:10.1002/2014GL060258.

Yoshida, T., Tanabe, T., Hirano, M., Muto, S., 2004. FT-IR study on the effect of OH content on the damage process in silica glasses irradiated by hydrogen. Nuclear Instruments and Methods in Physics Research B 218, 202–208. doi:10.1016/j.nimb.2003.12.056.

Zeller, E.J., Ronca, L.B., Levy, P.W., 1966. Proton-Induced Hydroxyl Formation on the Lunar Surface. J. Geophys. Res. 71, 4855. doi:10.1029/JZ071i020p04855.

Zhu, C., Crandall, P.B., Gillis-Davis, J.J., Ishii, H.A., Bradley, J.P., Corley, L.M., Kaiser, R.I., 2019. Untangling the formation and liberation of water

in the lunar regolith. Proceedings of the National Academy of Science 116, 11165–11170. doi:10.1073/pnas.1819600116.

Zhu, Y., Fu, X., Zhang, F., Zheng, Y., Zou, Y., 2014. Mineral surface modification induced by low energy ion irradiation: Implications for solar-wind exposure effects in lunar soil. Chin. J. Geochem. 33, 351–356. doi:10.1007/s11631-014-0697-8.

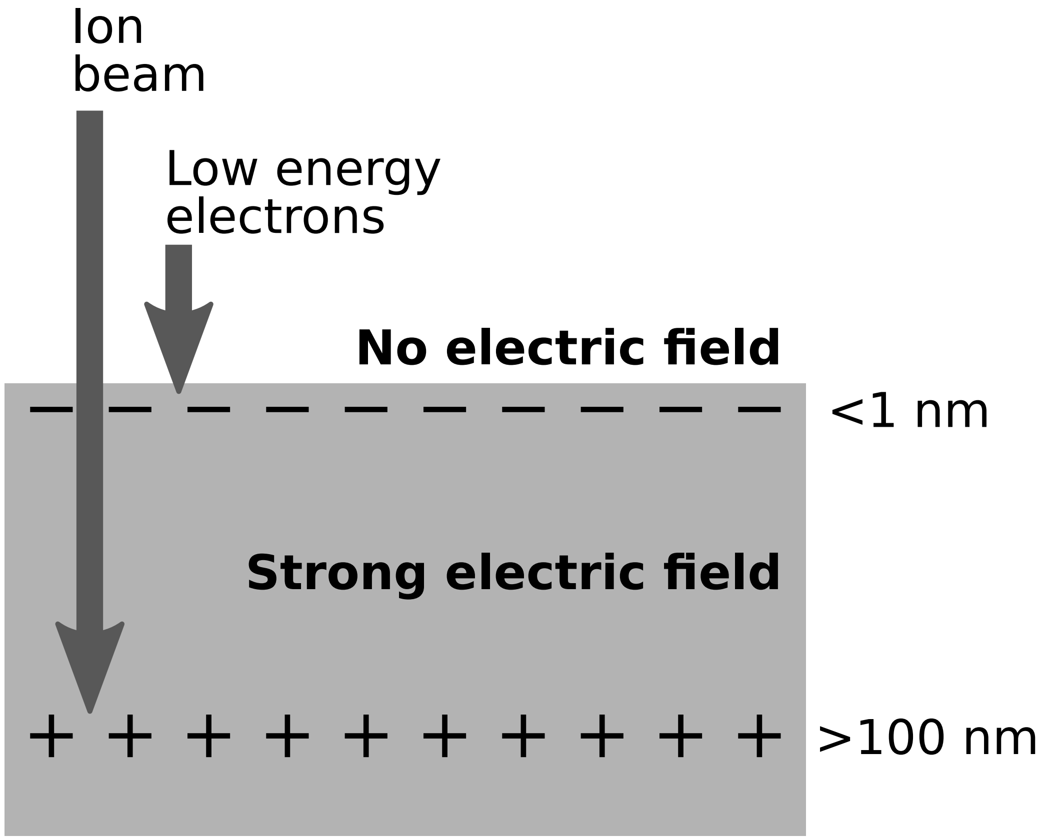

Figure 1: Cartoon showing how an electron flood gun and ion beam may keep a sample neutral, while still creating a strong interior electric field. It is not known how different the penetration depths of the two species must be before neutralization is too slow to prevent internal differential charging and potentially breakdown.

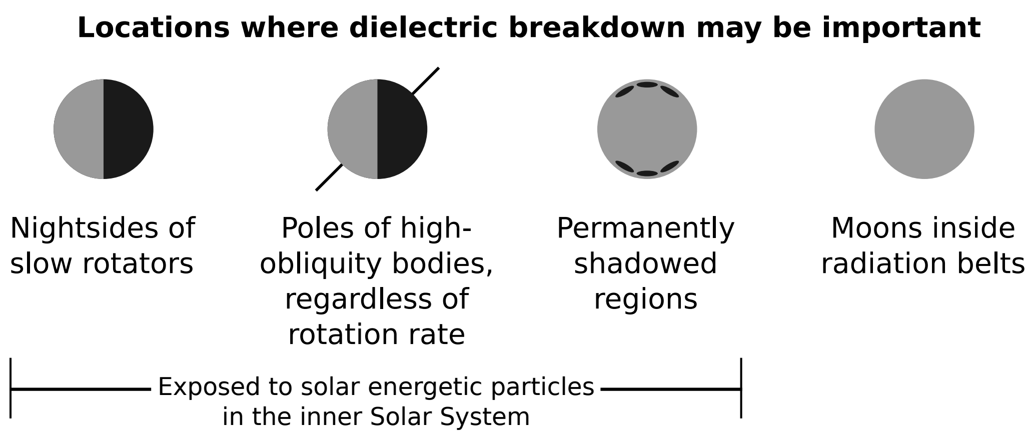

Figure 2: Illustration of the two sources of dielectric breakdown considered in this paper (solar energetic particles and radiation belts) and of the locations where breakdown may occur.